Arch. Metall. Mater. **62** (2017), 1, 137-140

DOI: 10.1515/amm-2017-0018

M. WOJCIECHOWSKA*[#], K. ZIEWIEC*, S. KĄC**, K. PRUSIK***

MECHANICAL PROPERTIES OF Ni-Fe-Cu-P-B ALLOY PRODUCED BY TWO COMPONENT MELT SPINNING (TCMS)

The aim of this work was to investigate the microstructure and mechanical properties of the two-component melt-spun (TCMS) alloy produced from $Ni_{40}Fe_{40}B_{20}$ and $Ni_{70}Cu_{10}P_{20}$ melts. The $Ni_{40}Fe_{40}B_{20,}$ $Ni_{70}Cu_{10}P_{20,}$ $Ni_{55}Fe_{20}Cu_{5}P_{10}B_{10}$ alloys were arc-melted. Then the alloys were melt-spun in the two different ways i.e.: by casting from a single-chamber crucible and from the two-chamber crucible. All of the above mentioned alloys were processed in the first way and the $Ni_{40}Fe_{40}B_{20}$ and $Ni_{70}Cu_{10}P_{20}$ were simultaneously cast on the copper roller from the two-chamber crucible. The microstructure of the alloy was studied using transmission electron microscopy (TEM), scanning electron microscopy (SEM) with energy dispersive spectrometry (EDS) and light microscopy. The mechanical properties were investigated using tensile testing and nanoindentation. The two-component melt-spun (TCMS) amorphous $Ni_{55}Fe_{20}Cu_{5}P_{10}B_{10}$ alloy present hardness, tensile strength and Young modulus on the significantly higher level than for a single phase amorphous $Ni_{55}Fe_{20}Cu_{5}P_{10}B_{10}$ alloy and slightly below the corresponding values for the $Ni_{40}Fe_{40}B_{20}$.

Keywords: metallic glasses, scanning electron microscopy (SEM), nanoindentation, transmission electron microscopy (TEM), mechanical properties.

1. Introduction

Metallic glasses are highly valued engineering material, among others due to their good mechanical properties, high magnetic permeability and interesting electrical properties. However, the lack of plasticity is serious disadvantage [1-2]. The possibility of improving the ductility of metallic glasses was examined in many works. The two-phase composite $Ni_{58.5}Nb_{20.25}Y_{21.25}$ alloy has better plasticity due to the addition of the second phase. The propagation of shear bands during deformation mainly initiates in the softer matrix, but it is interrupted or deflected when they collide with the globular harder phase [3]. Another alloy improved by precipitations of the second phase is $(Zr_{48}Cu_{36}Ag_{8}Al_{8})_{90}Ta_{10}$. The addition of 10% Ta increase plastic strain from 0.1% to 31% of this alloy [4]. However, the size of the precipitates of second phase in these alloys is diversified and the ability to produce such materials is limited only to a group of alloys, consisting mostly of rare earth elements.

There is a new technique for production of amorphous composites which overcomes limitations listed above [5-7]. Two component melt spinning enables obtaining composite amorphous/amorphous alloys consisting of thin bands of glassy phases of the differentiated chemical composition. Composites produced in this way are also characterized by a ductile fracture. The aim of this work is show interesting microstructure and mechanical properties of the two-component melt-spun (TCMS) alloy produced from $Ni_{40}Fe_{40}B_{20}$ and $Ni_{70}Cu_{10}P_{20}$ melts.

2. Experimental

Three-component alloys: $Ni_{40}Fe_{40}B_{20}$, $Ni_{70}Cu_{10}P_{20}$ and five-component alloy $Ni_{55}Fe_{20}Cu_{5}P_{10}B_{10}$ were prepared starting from pure elements 99.95 wt. % Ni, 99.95 wt. % Fe, 99.95 wt. % Cu, Ni-P, Cu-P, Ni-B, and Fe-B master alloys. The precursors were arc-melted under argon titanium gettered atmosphere. Then the alloys were melt-spun in helium atmosphere at 40 m/s and ejection pressure of 150 kPa. The crucible orifice diameter was 1.2 mm. The four alloys were ejected on the roller. Three ribbons produced from $Ni_{40}Fe_{40}B_{20}$, $Ni_{70}Cu_{10}P_{20}$ and $Ni_{55}Fe_{20}Cu_{5}P_{10}B_{10}$ alloys were obtained by ejection after re-melting in a single-chamber crucible and then ejected into the copper roller. However, the ribbon of the $Ni_{55}Fe_{20}Cu_{5}P_{10}B_{10}$ nominal composition was obtained also by two component melt spinning (TCMS) of the $Ni_{40}Fe_{40}B_{20}$ and $Ni_{70}Cu_{10}P_{20}$ liquid alloys (Fig. 1). The microstructure and phase analysis of the TCMS sample was investigated using JEOL 300 kV transmission electron microscope (TEM). Cross-section microstructure of the TCMS $Ni_{55}Fe_{20}Cu_{5}P_{10}B_{10}$ ribbon was observed by scanning electron microscope (SEM) with EDS JEOL 6610 and light microscope (LM) OLYMPUS GX51.

Nanoindentation tests were performed on mounted and polished cross-section of the ribbons, using a Nanoindenter NHT 50-183 with a diamond Berkovich-type indenter. The measurements are performed using a following parameters: constant loading rate of 100 μN/min to a maximum force of 50 μN, held

* INSTITUTE OF TECHNOLOGY, FACULTY OF MATHEMATICS, PHYSICS AND TECHNICAL SCIENCE, PEDAGOGICAL UNIVERSITY OF CRACOW, 2. PODCHORĄŻYCH STR., 30-084 KRAKÓW, POLAND
** AGH UNIVERSITY OF SCIENCE AND TECHNOLOGY, FACULTY OF METALS ENGINEERING AND INDUSTRIAL COMPUTER SCIENCE, AL. MICKIEWICZA 30, 30-059 KRAKÓW, POLAND
*** FACULTY OF COMPUTER SCIENCE AND MATERIALS SCIENCE, UNIVERSITY OF SILESIA,. 1A. 75 PUŁKU PIECHOTY STR., 41-500 CHORZÓW, POLAND

[#] Corresponding author: mirwoj@up.krakow.pl

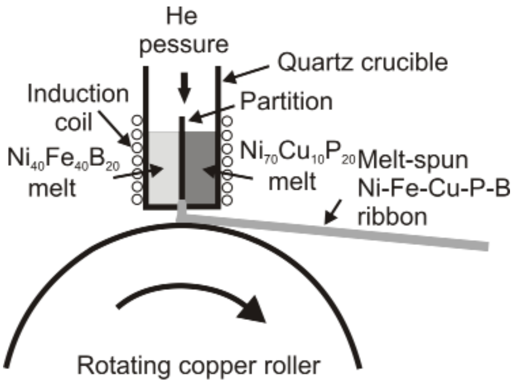

Fig. 1. Scheme of two component melt spinning (TCMS) technique

during 10 s followed by unloading at a constant rate of 100 μN/min. The hardness and Young modulus were derived from load-displacement curves in accordance with Oliver and Pharr method [8]. After the tests, traces of the indenter were examined by scanning electron microscope with EDS JEOL 6610. The tensile tests of the ribbons were performed. The specimens with a gauge length of 20 mm, a width of 2.4 mm, and a thickness of 23 μm ± 6 μm were prepared, and tested at room temperature at a crosshead speed of 1 mm/min. Following the tensile tests, the fractures of the $Ni_{55}Fe_{20}Cu_5P_{10}B_{10}$ TCMS ribbon as well as the $Ni_{40}Fe_{40}B_{20}$, $Ni_{70}Cu_{10}P_{20}$, and $Ni_{55}Fe_{20}Cu_5P_{10}B_{10}$ ribbons melt-spun from a single chamber crucible were characterized by means of a scanning electron microscope with EDS JEOL 6610.

3. Results and discussion

TEM microstructure of the TCMS $Ni_{55}Fe_{20}Cu_5P_{10}B_{10}$ alloy is presented in Figure 2a. The microstructure of this ribbon shows darker bands marked as "A" and brighter bands marked as "B" (Fig. 2a). Electron diffraction pattern in Figure 2b shows broad diffusive ring. This proves that the TCMS alloy has amorphous structure. One strong diffusive ring is located in the position which corresponds to the range of values between 1.9 Å and 2.3 Å. Different of contrast between areas "A" and "B" as shown in the microstructure of the two-component melt-spun alloy, may be due to the content of the species having different atomic numbers. Thus, the "A" areas are darker because they contain more Ni (Z = 28) and Cu (Z = 29) and "B" areas are enriched in Ni (Z = 28) and Fe (Z = 26).

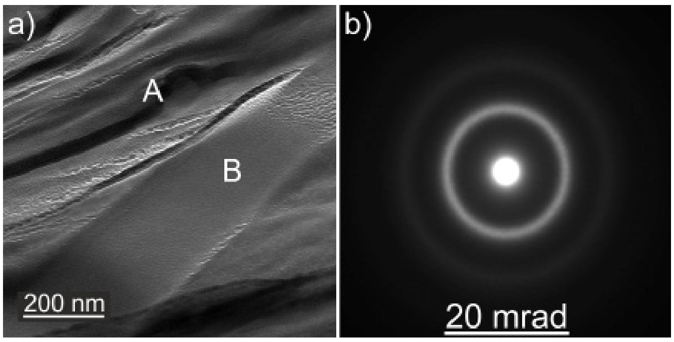

Fig. 2. TEM microstructure of TCMS $Ni_{55}Fe_{20}Cu_5P_{10}B_{10}$ alloy (a) and electron diffraction pattern (b)

Cross-section microstructure of TCMS $Ni_{55}Fe_{20}Cu_5B_{10}P_{10}$ ribbon and results of EDS analysis is presented in Figure 3. EDS line scan is defined as white line on SEM image (Fig. 3a) and as white arrows on LM image (Fig. 3b). Figure 3b presents lamellar microstructure of TCMS $Ni_{55}Fe_{20}Cu_5B_{10}P_{10}$ ribbon ejected by two component melt spinning (TCMS) from the $Ni_{40}Fe_{40}B_{20}$ and $Ni_{70}Cu_{10}P_{20}$ liquid alloys. Results of EDS analysis (Fig. 3c) show that the bands visible on LM image (Fig. 3b) have differentiated chemical composition. The darker bands are enriched in Ni, Cu and P but brighter bands mainly contain Fe. Boron content was not analyzed, but it is expected that the brighter areas are also enriched in B. Obviously, the fluxes of $Ni_{40}Fe_{40}B_{20}$ and $Ni_{70}Cu_{10}P_{20}$ liquid alloys were slightly mixed while passing through the orifice in the crucible. However, rapid cooling during the melt spinning process did not lead to complete mixing and homogenization of the alloys. It allowed to obtain a lamellar microstructure, composed of bands of Ni-Fe-B and Ni-Cu-P alloys.

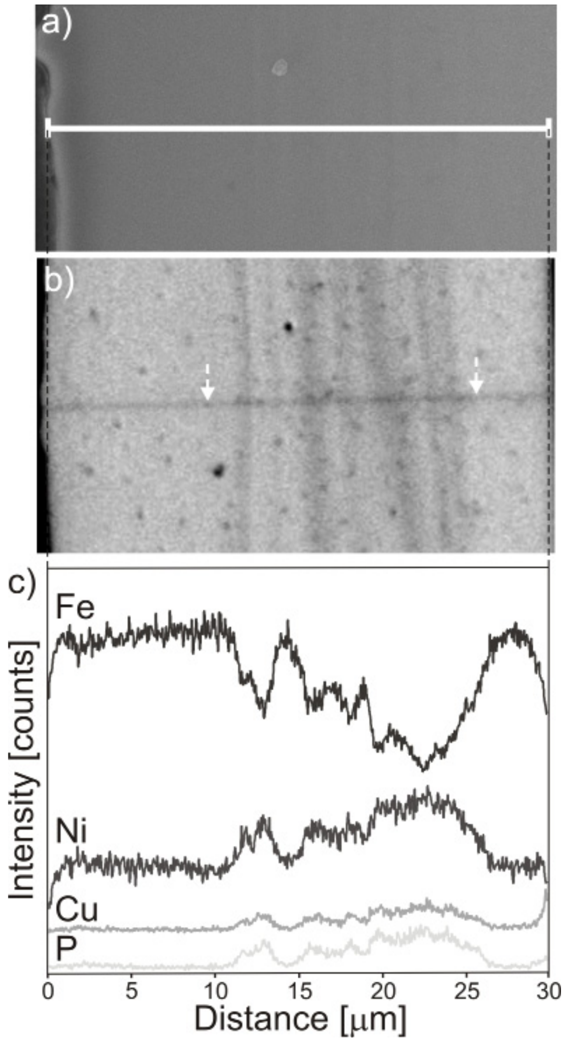

Fig. 3. Microstructure of TCMS $Ni_{55}Fe_{20}Cu_5B_{10}P_{10}$ ribbon with results of EDS analysis; a) SEM image with EDS line scan; b) Light microscope image with EDS line scan determined by white arrows; c) EDS results of line marked on (a) and (b)

The observation performed using TEM and SEM confirm that the microstructure of TCMS $Ni_{55}Fe_{20}Cu_5B_{10}P_{10}$ ribbon has a lamellar wood-like morphology, consisting of brighter and darker amorphous bands of the differentiated chemical composition that probably correspond to the Ni-Cu-P and Ni-Fe-B alloys.

Figure 4 presents load-displacement nanoindentation curves of all studied alloys and EDS maps of $Ni_{55}Fe_{20}Cu_5P_{10}B_{10}$ ribbons ejected from single-chamber and double-chamber crucible (Fig. 4b). Due to the weak contrast, the indentation places were marked by triangles. The values of Hardness (H) and Young modulus (E) are presented in Figures 5a, 5c and in Table 1. Load-displacement curves (Fig. 4a) and the values received from the nanoindentation test (Fig. 5a, 5c, Table 1) show that the highest hardness and Young modulus are obtained for $Ni_{40}Fe_{40}B_{20}$ alloy, i.e.: $H = 961$ HV, $E = 176$ GPa, respectively. Considerably lower H and E values are obtained for the remaining ribbons melt-spun from the single-chamber crucible, i.e.: $Ni_{70}Cu_{10}P_{20} - H = 620$ HV, $E = 114$ GPa, and $Ni_{55}Fe_{20}Cu_5P_{10}B_{10} - H = 575$ HV, $E = 108$ GPa. Hardness of two-component melt-spun $Ni_{55}Fe_{20}Cu_5B_{10}P_{10}$ ribbon is $H = 724$ HV and Young modulus $E = 141$ GPa. The results of EDS analysis (Fig. 4b) show lamellar microstructure of TCMS $Ni_{55}Fe_{20}Cu_5B_{10}P_{10}$ ribbon. Bands enriched in Fe also contain Ni, in turn bands enriched in Ni, contain Cu and P. This results proves that microstructure of TCMS amorphous composite is composed of bands of Ni-Fe-B and Ni-Cu-P alloys.

The results of the tensile tests presented in Figures 5b, 5c, 6 and Table 1 show that the highest tensile strength and Young modulus are obtained for the $Ni_{40}Fe_{40}B_{20}$ alloy, i.e.: $R_m = 2055$ MPa, $E = 152$ GPa, respectively. Substantially lower

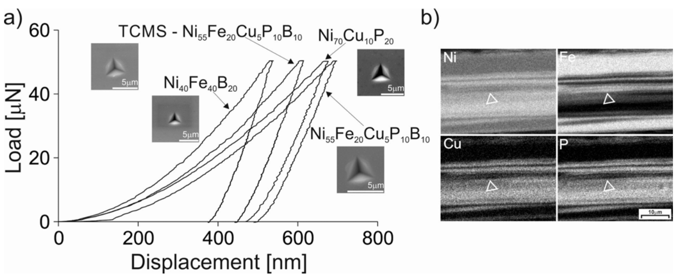

Fig. 4. Load-displacement curves measured during nanoindentation tests a) for $Ni_{40}Fe_{40}B_{20}$, TCMS $Ni_{55}Fe_{20}Cu_5P_{10}B_{10}$, $Ni_{70}Cu_{10}P_{20}$, $Ni_{55}Fe_{20}Cu_5P_{10}B_{10}$ amorphous alloys with EDS results for b) TCMS $Ni_{55}Fe_{20}Cu_5P_{10}B_{10}$ ribbons; triangles on EDS maps determine the trace of the intender

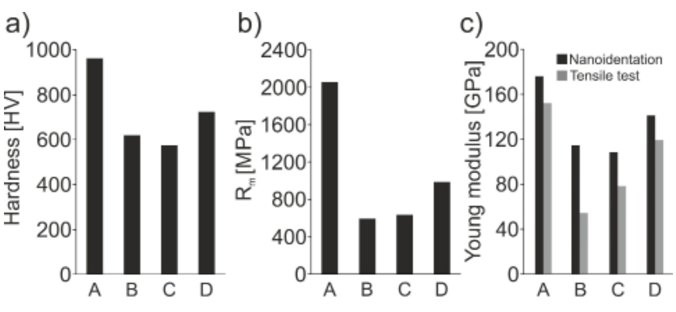

Fig. 5. Values of a) Hardness, b) Tensile strength (R_m) and c) Young modulus of A-$Ni_{40}Fe_{40}B_{20}$, B-$Ni_{70}Cu_{10}P_{20}$, C-$Ni_{55}Fe_{20}Cu_5B_{10}P_{10}$ and D-TCMS $Ni_{55}Fe_{20}Cu_5B_{10}P_{10}$ amorphous alloys

TABLE 1

Values of hardness, Young modulus and tensile strength of $Ni_{40}Fe_{40}B_{20}$, $Ni_{70}Cu_{10}P_{20}$, $Ni_{55}Fe_{20}Cu_5B_{10}P_{10}$ and TCMS $Ni_{55}Fe_{20}Cu_5B_{10}P_{10}$ amorphous alloys

Alloy	Nanoindentation test		Tensile test	
	Hardness [HV]	**Young modulus, *E* [GPa]**	**Tensile strength, R_m [MPa]**	**Young modulus, *E* [GPa]**
$Ni_{40}Fe_{40}B_{20}$	961	176	2055	152
$Ni_{70}Cu_{10}P_{20}$	620	114	592	54
$Ni_{55}Fe_{20}Cu_5P_{10}B_{10}$	575	108	634	78
TCMS $Ni_{55}Fe_{20}Cu_5B_{10}P_{10}$	724	141	985	119

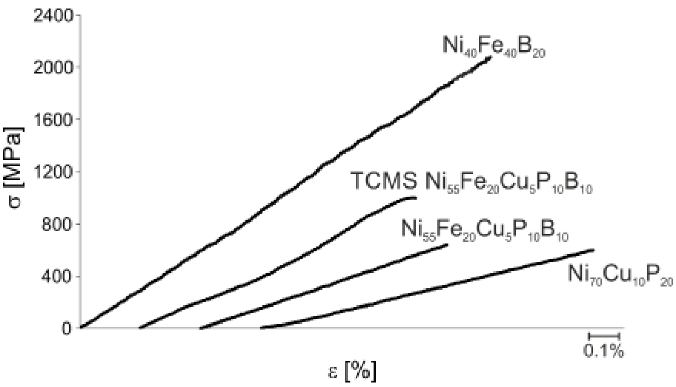

Fig. 6. Stress-strain ($\sigma - \varepsilon$) curves of $Ni_{40}Fe_{40}B_{20}$, $Ni_{70}Cu_{10}P_{20}$, $Ni_{55}Fe_{20}Cu_5P_{10}B_{10}$ and TCMS $Ni_{55}Fe_{20}Cu_5P_{10}B_{10}$ amorphous alloys

R_m and E values are obtained for the another ribbons ejected from the single-chamber crucible, i.e.: $Ni_{70}Cu_{10}P_{20} - R_m = 592$ MPa, $E = 54$ GPa, and $Ni_{55}Fe_{20}Cu_5P_{10}B_{10}$ $R_m = 634$ MPa, $E = 78$ GPa. For all of the above mentioned alloys $\sigma - \varepsilon$ linear relationships without apparent plastic deformation are observed. However, the TCMS $Ni_{55}Fe_{20}Cu_5P_{10}B_{10}$ $\sigma - \varepsilon$ plot just before breaking presents plastic deformation. Tensile strength of the alloy is $R_m = 985$ MPa, and Young modulus is $E = 119$ GPa.

Homogeneous alloys: $Ni_{40}Fe_{20}B_{20}$, $Ni_{70}Cu_{10}P_{20}$, which were used for producing the TCMS ribbon have significantly different mechanical properties. Hardness, Young modulus and tensile strength of $Ni_{40}Fe_{20}B_{20}$ ribbon is significantly higher than obtained for $Ni_{70}Cu_{10}P_{20}$ alloy. However, mechanical properties of two-component melt-spun ribbon are lower than $Ni_{40}Fe_{20}B_{20}$ and higher than $Ni_{70}Cu_{10}P_{20}$ alloy. Values of hardness and Young modulus of TCMS $Ni_{55}Fe_{20}Cu_5P_{10}B_{10}$ ribbon are also near to the average values obtained for $Ni_{40}Fe_{20}B_{20}$ and $Ni_{70}Cu_{10}P_{20}$ alloys. Moreover, the $\sigma - \varepsilon$ curve of TCMS ribbon as opposed to other studied alloys, shows plasticity. Hardness, Young modulus and tensile strength obtained for TCMS ribbon are also higher than for $Ni_{55}Fe_{20}Cu_5B_{10}P_{10}$ alloy ejected from single-chamber crucible. These results are confirm that two-phase structure of TCMS ribbon has improved the mechanical properties and plasticity of the alloy in comparison with single-phase alloys. The obtained results are also in accordance with the results of Consustell [3].

The main reason for the differentiation of Young modulus values obtained using nanoindentation and tensile test is that the nanoindentation test is local method and tensile test involves

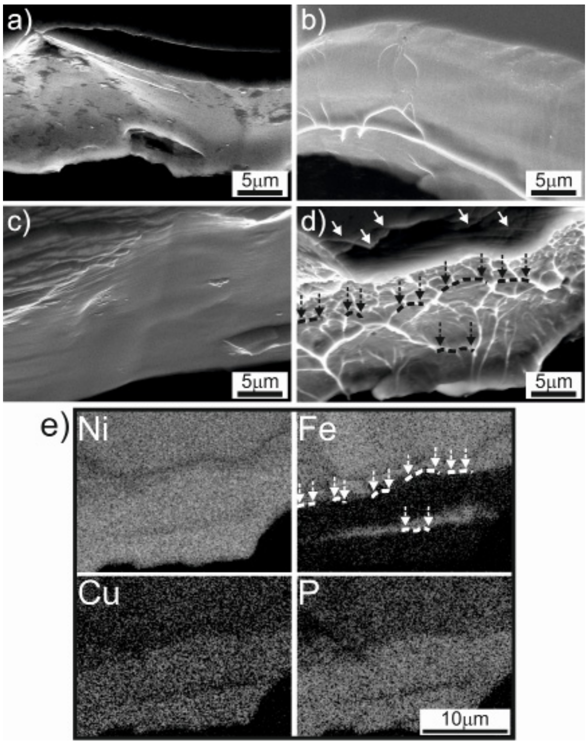

Fig. 7. SEM images of the fractures after tensile breaking of alloys: a) $Ni_{40}Fe_{40}B_{20}$; b) $Ni_{70}Cu_{10}P_{20}$; c) $Ni_{55}Fe_{20}Cu_5P_{10}B_{10}$; d) TCMS $Ni_{55}Fe_{20}Cu_5P_{10}B_{10}$; e) EDS maps showing the distribution of Ni, Fe, Cu, and P for the SEM image from (d); dotted lines and white arrows indicate the coincidence between the lamellar microstructure (d) and the boundaries of the $Ni_{40}Fe_{40}B_{20}$ and $Ni_{70}Cu_{10}P_{20}$ areas

more volume of the sample. Furthermore, the stress distribution at the nanoindenter is complex compared with the much simpler stress distributions for the macroscopic tensile test [9]

Tensile fractures of $Ni_{40}Fe_{40}B_{20}$, $Ni_{70}Cu_{10}P_{20}$, and $Ni_{55}Fe_{20}Cu_5B_{10}P_{10}$ and TCMS $Ni_{55}Fe_{20}Cu_5B_{10}P_{10}$ alloys are presented in (Fig. 7a-d), respectively. Fractures of $Ni_{40}Fe_{40}B_{20}$, $Ni_{70}Cu_{10}P_{20}$, and $Ni_{55}Fe_{20}Cu_5B_{10}P_{10}$ (Fig. 5a-c) ribbons ejected from single-chamber crucible are smooth, showing the fragility of the glassy alloys. This is connected with plastic flow in the form of a single shear bands, which is consistent with observation of Spaepen [10]. However, the fracture of the TCMS $Ni_{55}Fe_{20}Cu_5P_{10}B_{10}$ (Fig. 7d) alloy ejected from double-chamber crucible has more developed surface than the $Ni_{55}Fe_{20}Cu_5P_{10}B_{10}$ alloy (Fig. 7c) produced by using traditional single-chamber crucible. There are many shear bands on a fracture (Fig. 7d) (marked by white arrows) which is typical for ductile materials [11]. It is associated with a band-like microstructure of the differentiated Ni-Fe-B/Ni-Cu-P chemical composition. EDS maps presented in Figure 7e show that segments of ductile fracture can be found in the boundaries between the bands of Ni-Fe-B and Ni-Cu-P alloys (marked by dotted lines and arrows). The observation proves that the differentiated chemical composition of the Ni-Fe-B and Ni-Cu-P bands influence the fracture formation in the TCMS $Ni_{55}Fe_{20}Cu_5P_{10}B_{10}$ alloy. It is in agreement with results of Concustell [3] where the spherical precipitations of the second phase located in the amorphous matrix improved ductility of Ni-Nb-Y alloy.

4. Conclusion

1. The results of TEM observations confirm that the TCMS $Ni_{55}Fe_{20}Cu_5P_{10}B_{10}$ is amorphous and it consists of bands with different chemical composition, whereas SEM observations and EDS analysis confirm that these bands correspond to $Ni_{70}Cu_{10}P_{20}$ and $Ni_{40}Fe_{40}B_{20}$ areas.
2. TCMS ribbon was produced from alloys of significantly different mechanical properties. Values of Young modulus, hardness and tensile strength of TCMS are intermediate between $Ni_{40}Fe_{40}B_{20}$ and $Ni_{70}Cu_{10}P_{20}$ alloys. Moreover, the TCMS $Ni_{50}Fe_{20}Cu_{10}B_{10}P_{10}$ presents mechanical properties on the significantly higher level than for a single phase amorphous $Ni_{55}Fe_{20}Cu_5P_{10}B_{10}$ alloy.
3. The unique microstructure of the TCMS alloy influences the formation of the ductile fracture that is related to the arrangement of the bands of the differentiated chemical composition. While the $Ni_{55}Fe_{20}Cu_5B_{10}P_{10}$ alloy ejected from single-chamber crucible presents brittle fracture, the special feature of the fracture found in the TCMS $Ni_{55}Fe_{20}Cu_5B_{10}P_{10}$ alloy is ductile appearance of the fracture, where ductile segments of the fracture coincide with the boundaries between the $Ni_{70}Cu_{10}P_{20}$ and $Ni_{40}Fe_{40}B_{20}$ bands.

Acknowledgments

The work described in this paper was supported by a grant from the National Science Centre (NCN) (project number 2012/05/B/ST8/02644).

REFERENCES

[1] M.F. Ashby, A.L. Greer, Scripta Materialia **54**, 321-326 (2006).
[2] W.H. Wang, Journal of Non-Crystalline Solids **351**, 1481-1485 (2005).
[3] A. Concustell, N. Mattern, U. Kühn, A. Gebert, T. Gemming, M. Zinkevich, H. Wendrock, L. Schultz, Scripta Materialia **56**, 85-88 (2007).
[4] Q. Zhang, W. Zhang, G. Xie, A. Inoue, International Journals of minerals, metallurgy and materials **17**, 2, 208-213 (2010).
[5] K. Ziewiec, K. Prusik, K. Bryła, A. Ziewiec, Solid State Phenomena **203-204**, 361-367 (2013).
[6] K. Ziewiec, A. Błachowski, K. Ruebenbauer, A Ziewiec, K. Prusik, J. Latuch, M. Zięba, K. Bryła, Journal of Alloys and Compounds **615**, S29-S34 (2014).
[7] M. Różycka, K. Ziewiec, A. Błachowski, K. Ruebenbauer, K. Prusik, Journal of Non-Crystalline Solids **412**, 49-52 (2015).
[8] W.C. Oliver, G. M. Pharr, Journal of Materials Research **19**, 1, 3-20 (2004)
[9] M. Iijima, T. Muguruma, W.A. Brantley, I. Mizoguchi, Am. J. Orthod. Dentofacial. Orthop., Jul **140**(1), 65-71 (2011).
[10] F. Spaepen, Acta Metall. **25**, 407-415 (1977).
[11] H.J. Leamy, H.S. Chen, T.T. Wang, Metallurgical Transactions **3**, 699-708 (1972).